

Experimental Demonstration of a Coherent Perfect Absorber with PT Phase Transition

Yong Sun,¹ Wei Tan,^{1,2} Hong-qiang Li,¹ Jensen Li,^{3,*†} and Hong Chen^{1,*‡}

¹Key Laboratory of Advanced Micro-structure Materials (MOE) and School of Physics Sciences and Engineering, Tongji University, Shanghai 200092, China

²Beijing Computational Science Research Center, Beijing 100084, China

³School of Physics and Astronomy, University of Birmingham, Birmingham B15 2TT, United Kingdom

(Received 30 June 2013; revised manuscript received 14 December 2013; published 10 April 2014)

We report the realization of a coherent perfect absorber, using a pair of passive resonators coupled to a microwave transmission line in the background, which can completely absorb light in its parity-time (PT)-symmetric phase but not in its broken phase. Instead of balancing material gain and loss, we exploit the incident waves in the open system as an effective gain so that ideal PT symmetry can be established by using only passive materials. Such a route will be effective to construct PT-symmetric metamaterials and also tunable PT-symmetric optical elements in general. It also provides a flexible platform for studying exceptional-point physics with both electric and magnetic responses.

DOI: 10.1103/PhysRevLett.112.143903

PACS numbers: 42.25.Bs, 78.20.Ci, 78.67.Pt

Parity-time (PT) symmetric optical systems have recently attracted tremendous attention for studying extraordinary physics of non-Hermitian Hamiltonians. It begins from a pioneering work in showing a PT-symmetric Hamiltonian has an entirely real-valued energy spectrum below a phase transition point [1,2]. In optics, a PT-symmetric potential is a complex refractive index profile satisfying $n(x) = n^*(-x)$, which for example, can be realized by a pair of coupled waveguides with balanced gain and loss [3–8]. A range of associated extraordinary phenomena have since been proposed, including novel beam refraction [4], power oscillation [5], loss-induced transparency [7], nonreciprocal Bloch oscillations [9], laser absorber [10,11], unidirectional invisibility [12–14] and various extraordinary nonlinear effects [15–17].

Due to the stringent requirement of balanced gain and loss in achieving an ideal PT symmetry, only a few of the above proposals have been realized experimentally [7,8,13]. As a remedy, we can resort to the nonideal PT symmetry in a passive system through an additional gauge transformation of the states or a mathematical biasing in the diagonal terms of the Hamiltonian [7,18]. However, an ideal PT-symmetric Hamiltonian is still preferred for its ability to reveal directly and prominently the various extraordinary phenomena associated with a PT phase transition or exceptional point.

Interestingly, a recent theoretical study suggested that an ideal PT symmetry can actually be established by using metamaterials with both electric and magnetic responses. Simulations have confirmed the PT-symmetric nature of such metamaterials [19]. Based on that work, here we implement such an idea by using electric and magnetic resonators coupled with a microwave transmission line in an open system. Such a system allows us to demonstrate ideal PT symmetry by using only passive materials while

the “matching” potential is realized by tuning the geometric parameters and the lumped resistance of the resonators. In this way, we are not only using an open system to probe the physical properties of a PT-symmetric potential, but also employing the incident waves in an open system as an effective gain. This effective gain, coming from the environment instead of materials, depends on the target observable optical phenomenon, which affects the way to formulate the effective Hamiltonian. In the experimental demonstration in this Letter, we balance the scattering loss and the dissipative loss of the resonators without requiring gain to obtain coherent perfect absorption in the PT-symmetric phase. A coherent perfect absorber has shown great promise for interferometric applications in optical circuits [10,11,20]. A PT phase transition will further add configurational tunability and may allow us to design future modulators and switches with physics enriched by phase transition and exceptional-point physics.

Figure 1 shows our coupled-resonators system to exhibit an ideal PT symmetry. It consists of a “bright” resonator, the vertical copper wire in Fig. 1(a), and a “dark” resonator, the pair of split rings in Fig. 1(c). The “bright” resonator with electric dipole moment p can be easily excited by incoming waves ($s_{1,\text{in}}$ and $s_{2,\text{in}}$ from the two ports labeled as 1 and 2 in the figure), while the “dark” resonator, the pair of split-rings being modeled as a magnetic dipole moment m , is isolated from the transmission line (in the combined system, Fig. 1(e)) and can only be excited by the near-field from the bright resonator through a coupling parameter g . The two modes satisfy the coupled mode equations using a Lorentz model (with time dependence $\exp(-i\omega t)$)

$$\begin{aligned} (-\omega^2 - 2i\omega(\Gamma_a + f_a) + \omega_0^2)p &= 2f_a(s_{1,\text{in}} + s_{2,\text{in}} - i\omega gm), \\ (-\omega^2 - 2i\omega\Gamma_b + \omega_0^2)m &= 2i\omega f_b gp, \end{aligned} \quad (1)$$

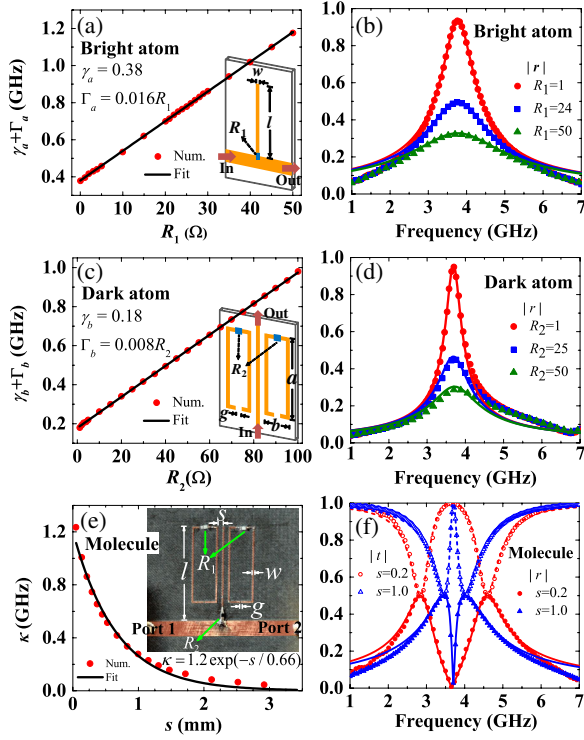


FIG. 1 (color online). Left column: simulated (red symbols) and fitted (solid line) total linewidth of bright (a) and dark resonator (c) as a function of lumped resistance. (e) Coupling strength as a function of separation between two resonators. Right column: simulated (symbols) and analytical (lines) transmission or reflection responses of bright resonator (b), dark resonator (d), and coupled structure (f) corresponding to the left column, with structural parameters given in Ref. [21].

and generate outgoing waves $s_{1,\text{out}}$ and $s_{2,\text{out}}$ at the two ports governed by

$$s_{1,\text{in}} - s_{2,\text{out}} = s_{2,\text{in}} - s_{1,\text{out}} = -i\omega p, \quad (2)$$

where f_a, f_b are the resonance strengths and Γ_a, Γ_b are the dissipative losses of the two individual resonators. The scattering loss for the bright resonator is also given by $\gamma_a = f_a$ while the scattering loss for the dark resonator is approximately zero. The dipole moments and the resonance strengths are normalized with respect to the transmission line environment [21]. The resonating frequencies for both resonators are tuned to the same ω_0 . Such a model and similar structures coupling bright and dark resonators are previously used for obtaining electromagnetic induced transparency and/or absorption [23–28] by working in the strong coupling regime and in the limit where the loss for the dark resonator is much smaller than the bright one: $\Gamma_b \ll \Gamma_a + \gamma_a$.

In contrast, here we work in the regime of intermediate coupling. Moreover, losses from the two resonators are specially tuned to have comparable sizes (as we shall see) to obtain coherent perfect absorption (CPA) and to display

the corresponding exceptional-point physics of PT symmetry. CPA is a particular set of solutions such that the incoming waves from the two ports are completely absorbed [10,11,20]. In this case, by putting zero outgoing waves: $s_{1,\text{out}} = s_{2,\text{out}} = 0$ into Eqs. (1) and (2) with a further approximation of the Lorentz model by $\omega_0^2 - \omega^2 \approx 2\omega(\omega_0 - \omega)$, we obtain an equivalent eigenfrequency problem in solving the CPA states:

$$\mathbf{H} \begin{pmatrix} p/\sqrt{f_a} \\ m/\sqrt{f_b} \end{pmatrix} = \omega \begin{pmatrix} p/\sqrt{f_a} \\ m/\sqrt{f_b} \end{pmatrix}, \quad (3)$$

where the effective Hamiltonian is

$$\mathbf{H} = \begin{pmatrix} \omega_0 - i(\Gamma_a - \gamma_a) & i\kappa \\ -i\kappa & \omega_0 - i\Gamma_b \end{pmatrix}, \quad (4)$$

and the coupling strength is defined by $\kappa = g\sqrt{f_a}\sqrt{f_b}$. We have established a Hamiltonian different from the one solving normal modes (or lasing, without incident waves) since CPA occurs in an open system with incident waves. By solving $\det(\mathbf{H} - \omega\mathbf{I}) = 0$, we can obtain the eigenfrequencies ω of \mathbf{H} as

$$\omega = \omega_0 + i\frac{\gamma_a - \Gamma_a - \Gamma_b}{2} \pm \sqrt{\kappa^2 - \left(\frac{\gamma_a - \Gamma_a + \Gamma_b}{2}\right)^2} \quad (5)$$

which needs to be real in order to have CPA occur.

For the case $\gamma_a - \Gamma_a = \Gamma_b$, \mathbf{H} is called an ideal PT-symmetric Hamiltonian. Both the diagonal and off-diagonal terms of \mathbf{H} form conjugate pairs, as a signature of a two-state PT-symmetric Hamiltonian [2,29]. It requires a positive $\gamma_a - \Gamma_a$, the difference between scattering and dissipative loss of the bright resonator. From the dynamic equations, we can see that this term is in fact renormalized from the original gain $-\gamma_a - \Gamma_a$ due to the presence of incident waves. The incident waves thus provide the additional power to turn this term to be positive. Therefore, it can be regarded as an effective gain (in the current context of CPA) but now it does not necessarily come from the actual material gain as in previous studies [7,8]. It paves a way to demonstrate ideal PT symmetry in a passive optical system in this work. With a PT-symmetric Hamiltonian, the phase transition can then be observed by varying the coupling κ across a critical value of $\kappa_c = \Gamma_b$. The eigenfrequencies of PT-symmetric \mathbf{H} have two real values in the PT-symmetric phase $\kappa > \Gamma_b$, giving CPA at two real frequencies $\omega_{1,2} = \omega_0 \pm \sqrt{\kappa^2 - \Gamma_b^2}$, and become a complex conjugate pair in the broken phase $\kappa < \Gamma_b$, suggesting perfect absorption cannot occur in this phase. For the more general case $\gamma_a - \Gamma_a \neq \Gamma_b$, \mathbf{H} is called a nonideal PT-symmetric Hamiltonian. All the eigenvalues are biased by a purely imaginary number (from Eq. (5)) so

that the eigenfrequencies cannot be real for $\kappa > \kappa_c$. For $\kappa < \kappa_c$, eigenvalues split in the imaginary part and one of them will cross the real frequency axis at $\kappa^2 = (\gamma_a - \Gamma_a)\Gamma_b$ to give CPA. Interestingly, although the nonideal case cannot have the whole branch or phase for CPA, CPA occurs at one of the imaginary branch at a fixed κ (at frequency ω_0). It is worth mentioning that this solution cannot be found in the previous nonideal PT-symmetric system without gain [8] except for the case $\kappa = 0$.

In the following, we focus on the experimental realization of CPA with phase transition in passive coupled-resonator system. The detailed configurations are described in the Supplementary Material [21]. According to the theoretical proposal, the loss rates of the bright and dark resonators as well as the coupling between them need to be carefully balanced in order to achieve CPA with PT phase transition. We first investigate the bright and the dark resonators separately to extract the parameters appearing in coupled mode equations. Lumped resistance R_1/R_2 are used to control the loss rates of the bright or dark resonator. Figures 1(a) and 1(c) present the relationship between the value of R_1/R_2 and the resonating linewidth of the bright/dark resonator, respectively. As is shown in the insets, the bright resonator is excited by the 50 Ω microstrip, and the dark resonator is excited by a 0.2 mm width microstrip in the center (The separation between SRR and the microstrip is 0.4 mm). The red dots are the simulated half width at half maximum of the absorption line, which fit the linear formula quite well. As examples, simulated spectra (symbols) of the amplitudes of reflection coefficient with the values of $R_1 = 1, 24, 50 \Omega$ and $R_2 = 1, 25, 50 \Omega$ are plotted in Figs. 1(b) and 1(d), respectively. As a comparison, the theoretical calculations with fitted parameters are also given [the lines in Figs. 1(b) and 1(d)]. Both resonators are resonantly excited around the frequency of $f_0 = 3.75$ GHz, and the calculated results are in good agreement with the simulations near f_0 . The small deviations between them in the nonresonance frequency region are mainly due to the present of the high-order resonating mode of the branch and the SRRs. It is known that the total linewidth could be divided into two parts: the scattering loss $\gamma_{a,b}$ and the dissipative loss $\Gamma_{a,b}$. For the present design, the part of dissipative loss is totally from the lumped resistor. Therefore, the scattering loss $\gamma_{a,b}$ is equal to the linewidth at $R_{1,2} = 0$, i.e. the intercept of the fitted linear formula. One can obtain that $\gamma_a \approx 0.38$ GHz, $\gamma_b \approx 0.18$ GHz, $\Gamma_a \approx 0.016R_1$, and $\Gamma_b \approx 0.008R_2$. It should be noted that γ_b here can only represent the coupling between the SRR and the 0.2 mm vertical microstrip. For the coupled structure shown in Fig. 1(e), the scattering loss of the SRRs becomes negligible due to the large separation between the SRRs and the microstrip.

The coupling strength κ between the two resonators is determined by the separation s between the branch and the SRR, and it can be obtained from the spectral response of

the coupled structure for $\Gamma_b = 0$, i.e. $R_2 = 0$. The relationship between κ and s is given in Fig. 1(e). The red dots are the half of the frequency separation of two poles in simulated transmission or reflection spectra ($R_1 = 24 \Omega$, $R_2 = 0$), which can fit a decaying exponential function of $\kappa = 1.2 \exp(-s/0.66)$ quite well. Figure 1(f) exhibits the simulated spectra (symbols) of the transmission/reflection with the values of $s = 0.2, 1.0$ mm, as well as the theoretical calculations with fitted parameters (lines), which shows good consistency with each other.

Based on the studies above, one can obtain the parametric evolution of the coupled structure for CPA (Fig. 2). For fixed $R_1 = 1 \Omega$, ideal PT-symmetric Hamiltonian can be achieved by choosing $R_2 = 45.5 \Omega$, with $\gamma_a - \Gamma_a = \Gamma_b$ satisfied. It is denoted by the black and blue vertical lines representing the CPA with ideal PT symmetry and the PT-broken phase, respectively. The threshold of coupling is at $s = 0.79$ mm. The splitting of the real/imaginary (black solid / red open circles) part of the eigenfrequency (relative to the original resonating frequency ω_0) of PT-symmetric \mathbf{H} with varying s is shown in the inset, as a typical ideal PT phase transition.

The structure with ideal PT symmetry is then excited by incident waves of $(s_{1+}, s_{2+}) = (1, 1)$, namely in-phase excitation with the same intensity from the two opposite

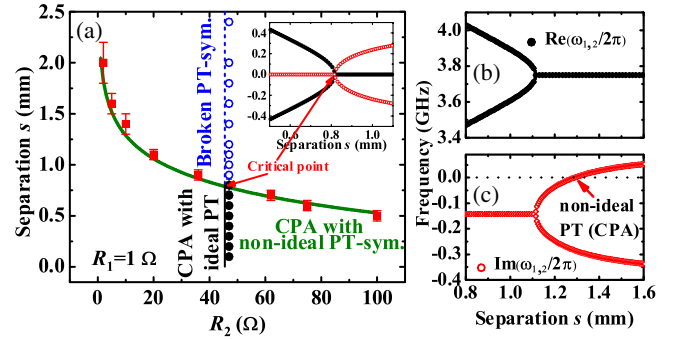


FIG. 2 (color online). (a) Phase map of the PT-symmetric Hamiltonian in passive structure. The vertical black solid line corresponds to the ideal PT symmetry with two split real eigenfrequencies, and the vertical blue dash line corresponds to the PT-broken phase. Curved solid green line shows the real eigenfrequency condition (to have CPA) at a nonideal PT symmetry. The black circles, blue open circles, and red squares denote the parameter settings of the experimental samples, with which CPA for the ideal PT symmetry, no CPA for the spontaneous PT-symmetry breaking, and CPA for the nonideal PT symmetry are, respectively, verified. Inset gives the eigenfrequencies (with respect to the original resonating frequency in GHz: real or imaginary part shown in black solid or red open circles) as a function of separation (coupling strength). The dependence of the eigenfrequencies of a nonideal PT-symmetric Hamiltonian at $R_2 = 10 \Omega$ against the coupling separation s is given in (b) real part and (c) the imaginary part. A pure real eigenfrequency to have CPA can be found at a particular separation.

directions. The magnitude of the coherent absorption equals to $1-|t+r|^2$, where t/r is the one-side transmission/reflection coefficient with respect to the mirror plane of the sample. In Fig. 3(a), we depict the measured coherent absorptions of a series of samples with different s . It is clearly seen that when s is smaller than 0.8 mm, there exist two CPA frequencies (coherent absorption coefficient being nearly 1) corresponding to the two real eigenfrequencies of PT-symmetric \mathbf{H} ; when s is larger than 0.8 mm, PT phase transition occurs, and no CPA frequency can be found. In Fig. 3(b), the analytical outgoing $|t+r|^2$ spectra (with $R_1 = 1$, $R_2 = 47 \Omega$ and fitted parameters) versus frequency and separation s are also plotted. One can find that the simulated (red solid circles) and measured (black open circles) CPA frequencies are in good agreement with the analytical results. These results confirm the theoretical model proposed above and demonstrate the ideal PT-symmetry behaviors in a passive system. Note that the coherent absorption of the structure were not measured directly in the experiments. Instead, we measured the one-side transmission and reflection spectra, and then obtained the coherent absorption. Moreover, the absorption efficiency at the two peaks in the PT-symmetric phase can be tuned by controlling the relative phase between the two inputs, with frequency positions fairly unchanged. (see Ref. [21] for additional simulated and measured spectra).

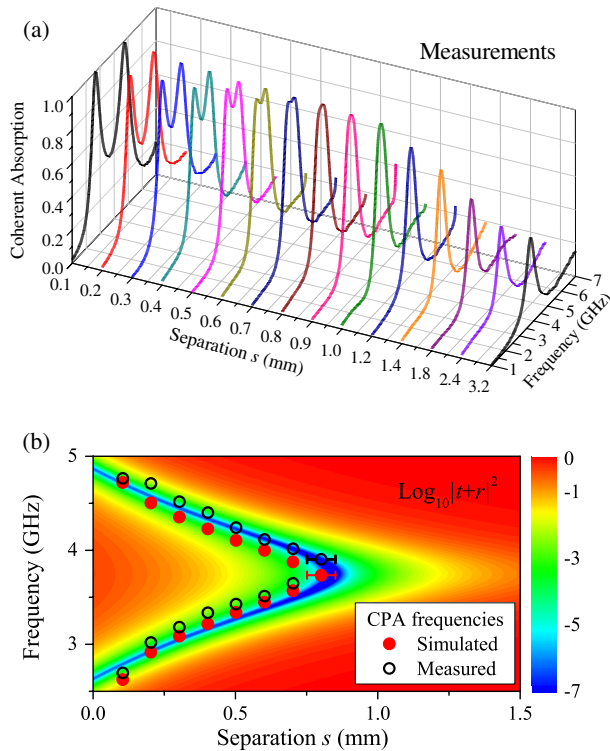


FIG. 3 (color online). Ideal PT symmetry. (a) Measured coherent absorption as a function of s . (b) Analytical outgoing spectra $|t+r|^2$ with varying s . The red solid and black open circles are the simulated and measured CPA frequencies, respectively.

CPA can also occur with nonideal PT-symmetric \mathbf{H} with specific loss-coupling relation, which is indicated by the green curve in Fig. 2. It suggests that a real eigenfrequency can also be achieved in nonideal PT-symmetric system. Here we construct nonideal PT-symmetric system with the resistor R_2 , which is either more than or less than 45.5Ω , and seek the CPA conditions (corresponding to real eigenvalue) by scanning the coupling strength (equivalently the separation s). For the case of ideal PT-symmetric \mathbf{H} , CPA can be observed with any separation smaller the threshold value; however, for nonideal PT-symmetric \mathbf{H} , CPA can only be observed at the center frequency of $f_0 = 3.75$ GHz, with a particular separation. The experimental CPA conditions of nonideal PT-symmetric system are presented in Fig. 2(a) with red squares. In Fig. 4, simulations and measurements show that the particular separations for the samples with $R_2 = 5, 10$, and 100Ω are near 1.6, 1.4, 0.5 mm, respectively. The CPA is characterized by a large dip at the center frequency of $f_0 = 3.75$ GHz (red solid line). Smaller or larger of the separation makes CPA disappear (blue dashed and black dotted lines). The measurements show good agreement with simulations, and verify the theoretical predictions.

In summary, we have experimentally demonstrated an ideal PT symmetry by balancing scattering and dissipative losses in a coupled-resonator system. Coherent perfect absorption is achieved with purely passive materials, while the associated PT phase transition is clearly observed. Such investigations will be useful for designing future tunable optical components benefiting from PT phase transition and exceptional-point physics. It is also expected the same route is immediately useful to construct a PT-symmetric microwave metamaterial with possible extension to higher frequencies.

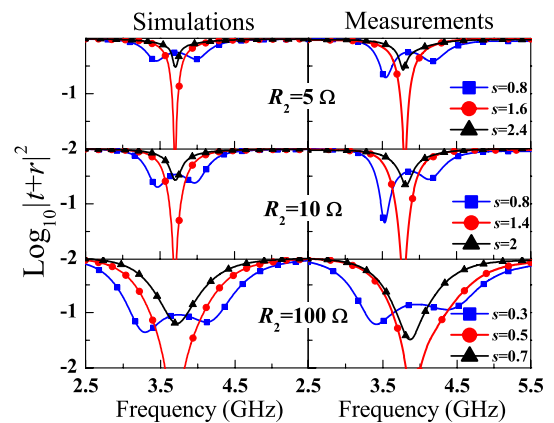


FIG. 4 (color online). Simulated and measured outgoing spectra of nonideal PT-symmetric system for three samples with $R_2 = 5, 10$, and 100Ω . The dips of the red curves indicate the CPA frequency of 3.75 GHz for their critical couplings; the blue and black curves show that CPA cannot be observed when the coupling strength is more or less than the critical coupling.

This research was supported by CNKBRFSF (Grant No. 2011CB922001) and by CNSF (Grants No. 11234010 and No. 11204217). J.L. would like to acknowledge funding support from the European Union's Seventh Framework Programme under Grant Agreement No. 630979.

*To whom all correspondence (inquiry) should be addressed.

[†]j.li@bham.ac.uk

[‡]hongchen@tongji.edu.cn

- [1] C. M. Bender and S. Boettcher, *Phys. Rev. Lett.* **80**, 5243 (1998); C. M. Bender, *Rep. Prog. Phys.* **70**, 947 (2007).
- [2] C. M. Bender, M. V. Berry, and A. Mandilara, *J. Phys. A* **35**, L467 (2002).
- [3] R. El-Ganainy, K. G. Makris, D. N. Christodoulides, and Z. H. Musslimani, *Opt. Lett.* **32**, 2632 (2007).
- [4] K. G. Makris, R. El-Ganainy, D. N. Christodoulides, and Z. H. Musslimani, *Phys. Rev. Lett.* **100**, 103904 (2008).
- [5] Z. H. Musslimani, K. G. Makris, R. El-Ganainy, and D. N. Christodoulides, *Phys. Rev. Lett.* **100**, 030402 (2008).
- [6] S. Klaiman, U. Günther, and N. Moiseyev, *Phys. Rev. Lett.* **101**, 080402 (2008).
- [7] A. Guo, G. J. Salamo, D. Duchesne, R. Morandotti, M. Volatier-Ravat, V. Aimez, G. A. Siviloglou, and D. N. Christodoulides, *Phys. Rev. Lett.* **103**, 093902 (2009).
- [8] C. E. Ruter, K. G. Makris, R. El-Ganainy, D. N. Christodoulides, M. Segev, and D. Kip, *Nat. Phys.* **6**, 192 (2010).
- [9] S. Longhi, *Phys. Rev. Lett.* **103**, 123601 (2009).
- [10] S. Longhi, *Phys. Rev. A* **82**, 031801(R) (2010).
- [11] Y. D. Chong, L. Ge, and A. D. Stone, *Phys. Rev. Lett.* **106**, 093902 (2011).
- [12] Z. Lin, H. Ramezani, T. Eichelkraut, T. Kottos, H. Cao, and D. N. Christodoulides, *Phys. Rev. Lett.* **106**, 213901 (2011).
- [13] A. Regensburger, C. Bersch, M.-A. Miri, G. Onishchukov, D. N. Christodoulides, and U. Peschel, *Nature (London)* **488**, 167 (2012).
- [14] L. Feng, Y.-L. Xu, W. S. Fegadolli, M.-H. Lu, J. E. B. Oliveira, V. R. Almeida, Y.-F. Chen, and A. Scherer, *Nat. Mater.* **12**, 108 (2013).
- [15] S. V. Dmitriev, A. A. Sukhorukov, and Yu. S. Kivshar, *Opt. Lett.* **35**, 2976 (2010).
- [16] H. Ramezani, D. N. Christodoulides, V. Kovanis, I. Vitebskiy, and T. Kottos, *Phys. Rev. Lett.* **109**, 033902 (2012).
- [17] N. Lazarides and G. P. Tsironis, *Phys. Rev. Lett.* **110**, 053901 (2013).
- [18] S. Bittner, B. Dietz, U. Gunther, H. L. Harney, M. Miski-Oglu, A. Richter, and F. Schafer, *Phys. Rev. Lett.* **108**, 024101 (2012).
- [19] M. Kang, F. Liu, and J. Li, *Phys. Rev. A* **87**, 053824 (2013).
- [20] Y. D. Chong, L. Ge, H. Cao, and A. D. Stone, *Phys. Rev. Lett.* **105**, 053901 (2010).
- [21] See Supplementary Material at <http://link.aps.org/supplemental/10.1103/PhysRevLett.112.143903>, which includes Ref. [22], for details on analytic model and additional results.
- [22] J. D. Jackson, *Classical Electrodynamics* (Wiley, New York, 1998), 3rd ed.. (Sections 9.2 and 9.3).
- [23] S. Zhang, D. A. Genov, Y. Wang, M. Liu, and X. Zhang, *Phys. Rev. Lett.* **101**, 047401 (2008).
- [24] N. Liu, L. Langguth, T. Weiss, J. Kästel, M. Fleischhauer, T. Pfau, and H. Giessen, *Nat. Mater.* **8**, 758 (2009).
- [25] P. Tassin, L. Zhang, Th. Koschny, E. N. Economou, and C. M. Soukoulis, *Phys. Rev. Lett.* **102**, 053901 (2009).
- [26] Y. Sun, H. Jiang, Y. Yang, Y. Zhang, H. Chen, and S. Y. Zhu, *Phys. Rev. B* **83**, 195140 (2011).
- [27] R. Taubert, M. Hentschel, J. Kastel, and H. Giessen, *Nano Lett.* **12**, 1367 (2012).
- [28] P. Tassin, L. Zhang, R. Zhao, A. Jain, T. Koschny, and C. M. Soukoulis, *Phys. Rev. Lett.* **109**, 187401 (2012).
- [29] In our chosen basis, the parity operator is $P = \begin{pmatrix} 0 & i \\ -i & 0 \end{pmatrix}$ with $P^2 = I$ and the time-reverse operator is $T = \begin{pmatrix} 1 & 0 \\ 0 & -1 \end{pmatrix} K$ where K is the complex conjugation operator.